




Research Article

Improving the Corrosion Resistance of NiNb-Based Bulk Metallic Glass through the Hot Compression

Abeer Abdullah Al Anazi ¹, Andrés Alexis Ramírez-Coronel,^{2,3,4,5} Rasha Fadhel Obaid,⁶ Abdullah Albaker ⁷, M. Abdulfadhil Gatea,⁸ and Seyed Mojtaba Mostafavi ⁹

¹Department of Mechanical Engineering, Australian University (AU), Kuwait City, Kuwait

²Azogues Campus Nursing Career, Health and Behavior Research Group (HBR), Psychometry and Ethology Laboratory, Catholic University of Cuenca, Cuenca, Ecuador

³University of Palermo, Buenos Aires, Argentina

⁴ADEPIN Research Group, National University of Education, Azogues, Ecuador

⁵Epidemiology and Biostatistics Research Group, CES University, Colombia

⁶Department of Biomedical Engineering, Al-Mustaqbal University College, Babylon, Iraq

⁷Department of Electrical Engineering, College of Engineering, University of Ha'il, Ha'il 81451, Saudi Arabia

⁸Technical Engineering Department, College of Technical Engineering, The Islamic University, Najaf, Iraq

⁹Department of Chemistry, Islamic Azad University Tehran Branch, Tehran, Iran

Correspondence should be addressed to Seyed Mojtaba Mostafavi; mostafavi@rosecal.com.au

Received 20 October 2022; Revised 30 November 2022; Accepted 31 March 2023; Published 14 April 2023

Academic Editor: Majid Samavatian

Copyright © 2023 Abeer Abdullah Al Anazi et al. This is an open access article distributed under the Creative Commons Attribution License, which permits unrestricted use, distribution, and reproduction in any medium, provided the original work is properly cited.

This paper aims to study and evaluate the corrosion resistance of $\text{Ni}_{55}\text{Nb}_{45}$ and $\text{Ni}_{55}\text{Nb}_{35}\text{Co}_5\text{Zr}_5$ bulk metallic glasses (BMGs) in an environment similar to proton exchange membrane fuel cells. Moreover, the hot compression process was carried out to find the effects of a thermomechanical treatment on the corrosion resistance. The X-ray diffraction (XRD) test indicated that the hot compression process led to formation of crystalline species in both samples; however, it was more pronounced in the $\text{Ni}_{55}\text{Nb}_{35}\text{Co}_5\text{Zr}_5$ alloy. It is suggested that the minor addition of Zr and Co facilitated the crystallization in the material. The polarization test unveiled that the hot compression deteriorated the corrosion resistance of the $\text{Ni}_{55}\text{Nb}_{45}$ alloy through the introduction of anomalous chemical interfaces. On the other hand, the hot deformation affected the $\text{Ni}_{55}\text{Nb}_{35}\text{Co}_5\text{Zr}_5$ alloy in a positive way, so that the corrosion behavior improved compared with its fully glassy state. It is suggested that the hot deformation induces some NiNb crystalline constituencies in the microstructure of $\text{Ni}_{55}\text{Nb}_{35}\text{Co}_5\text{Zr}_5$ BMG, leading to the enrichment of glassy matrix from Zr/Co constituencies and the enhancement of corrosion resistance.

1. Introduction

In recent years, a growing interest has been attracted to apply bulk metallic glasses (BMGs) as the bipolar plates in the proton exchange membrane fuel cells [1–3]. A wide range of properties from corrosion resistance to flexural strength is needed for considering a material as a bipolar plate [4–6]. Among a broad spectrum of alloy compositions in the glassy systems, Ni-based BMGs are promising alloys with excellent corrosion resistance, which can be employed as bipolar

plates in the proton exchange membrane fuel cells [7, 8]. Several processes such as annealing, microalloying, and thermomechanical treatments have been carried out to improve the corrosion resistance of Ni-based BMGs as much as possible. For instance, Espinoza Vazquez et al. [9] reported that NiNb amorphous alloy exhibited a superior corrosion resistance under the presence of chloride ions when the pH value was in the range of 0–7. On the other hand, the passive film got inhomogeneous, and the corrosion rate increased at pH = 14. Zhao et al. [10] applied cryogenic

cycling and annealing treatments to improve the corrosion behavior of $\text{Ni}_{62}\text{Nb}_{33}\text{Zr}_5$ BMG in a 3.5 wt.% NaCl solution. Their results indicated that both treatments with optimized parameters enhanced the corrosion resistance and thermal stability. After cryogenic cycling, the sample exhibited an excellent corrosion resistance, which was related to the high degree of amorphization. In the annealed samples, the fully crystallized state showed a superior anticorrosion performance, which was due to the formation of Nb-rich and Zr-rich oxides. Poddar et al. [11] demonstrated that the oxidation kinetics of $\text{Ni}_{60}\text{Nb}_{30}\text{Ta}_{10}$ BMG included a two-stage parabolic-rate trend under the glass transition temperature. Moreover, the constant of the parabolic rate enhanced with the rise of oxidation temperature. Poddar et al. [12] also characterized the corrosion resistance of thermally oxidized $\text{Ni}_{60}\text{Nb}_{30}\text{Ta}_{10}$ in the nitric acid medium and found that the electrochemical corrosion behavior was consistent with the type of semiconducting nature of the oxide film. Reported in another study [13], it was unveiled that the amorphous $\text{Ni}_{60}\text{Nb}_{30}\text{Ta}_{10}$ exhibited a higher corrosion resistance in comparison with partially crystallized state. This was due to the depletion of the nano α -Ni phase in the system. Jiang et al. [14] applied NiNb amorphous coatings on the stainless steel for improving the corrosion resistance. It was unveiled that the $\text{Ni}_{50}\text{Nb}_{50}$ resisted corrosion owing to the creation of the passive film with a considerable amount of Nb_2O_5 species. On the other hand, the $\text{Ni}_{60}\text{Nb}_{40}$ amorphous coating with a high Ni content exhibited weak corrosion resistance owing to the devastation of the coating structure caused by the dissolution of Ni cations. Another investigation showed that the oxidation of $\text{Ni}_{50}\text{Zr}_{25}\text{Nb}_{25}$ BMG at 400°C led to the formation of an amorphous oxide film with species of ZrO_2 and Nb_2O_5 , improving the corrosion resistance in the concentrated nitric acid [15].

In general, the previous works indicated that the NiNb-based BMGs are promising alloys for application in corrosive environments [16–18]. However, it is possible to improve the corrosion resistance of this type of alloy through manipulating the chemical composition and applying mechanical or thermal treatments. For example, Wang et al. [19] unveiled that the heat treatment above the glass transition temperature significantly changed the corrosion resistance of the $\text{Zr}_{56}\text{Al}_{16}\text{Co}_{28}$ alloy. Zhao et al. [20] also reported that the corrosion behavior of the deformed ZrCuNiAl MG after heat treatment is much better than that of the deformed MG prior to the heat treatment. Figueira et al. [8] demonstrated that the thermomechanical post-treatment was an efficient method for improving the corrosion resistance of NiNb-based BMGs. It was also found that the severe surface deformation led to an alteration of free volume and enhancement of bio-corrosion resistance in the BMGs [21]. Xing et al. [22] indicated that the pre-compression treatment at room temperature induced the partial crystallization in the MGs and increased the corrosion resistance in the seawater solution. In this study, we added Zr and Co constitutes to the NiNb BMG and also conducted a thermomechanical process to enhance the corrosion resistance of NiNb BMGs in an environment similar to that of proton exchange membrane fuel cells

(PEMFC). In this type of cells, electricity is generated through a reaction between hydrogen and oxygen, so that the only by-products are water and heat [23, 24].

2. Experimental Procedure

The $\text{Ni}_{55}\text{Nb}_{45}$ and $\text{Ni}_{55}\text{Nb}_{35}\text{Co}_5\text{Zr}_5$ alloying compositions (at. %) were prepared through the arc-remelting process. To fabricate ingots with a homogeneous composition, high-purity elemental constituents (>99.7%) were mixed and melted for four times. The alloys were then cast using the water-cooled copper mold. The prepared samples were in the form of plates with dimensions of $40 \times 30 \times 2 \text{ mm}^3$. The temperature features of samples were characterized by a Perkin Elmer 6000 differential scanning calorimeter (DSC) with heating and cooling rates of 20 K/min under a protective environment. It should be noted that the DSC instrument was calibrated through the thermographs of high-purity Al and Zr elements. To apply thermomechanical treatment, the hot deformation was carried out at a 0.75 mm/min compression rate at $0.98T_g$. The final thickness of samples decreased about 2% after the hot deformation. The X-ray diffraction (XRD-EQUINOX 100) test with Cu-K α radiation was also carried out to reveal the amorphous structure or possible crystalline species in the samples.

To measure the electrochemical parameters, an Origa-Stat200 potentiostat was used along with a saturated Ag/AgCl electrode as reference and a platinum mesh as a counter-electrode. To simulate the environment of proton exchange membrane fuel cells, 2 ppm F + 1 M H_2SO_4 at 70°C were prepared [8, 25]. Prior to any measurement, the working electrode was left at open circuit potential for 2 hours. Electrochemical impedance microscopy was done with a signal amplitude around the open circuit potential and the recording rate of 15 points/decade. The curves of potentiodynamic polarization were obtained with the scan rate of 1 mV/s. It should be noted that the stainless steel 316L was considered as a reference material for comparative study.

3. Results and Discussion

At the first step, it is required to identify the possible formation of crystalline phases in the samples. Figure 1 illustrates the XRD patterns of $\text{Ni}_{55}\text{Nb}_{45}$ and $\text{Ni}_{55}\text{Nb}_{35}\text{Co}_5\text{Zr}_5$ at the initial and treated states. Considering the broad peak in the patterns, it is found that the samples at their initial state exhibit a dominant amorphous structure, implying that the copper mold casting successfully produced the BMGs. On the other hand, the thermomechanical process led to the formation of crystalline species in the samples. Although the types of crystals are similar for both alloy compositions, i.e., Ni_3Nb and Nb_7Ni_6 , the peak intensities in the XRD pattern of $\text{Ni}_{55}\text{Nb}_{35}\text{Co}_5\text{Zr}_5$ are obviously sharper. This result indicates that the minor addition of Zr and Co facilitates the formation of NiNb crystalline phases under hot compression. To ascertain the reasons for this event, it is necessary to evaluate the thermographs of samples. Figure 2(a) represents the DSC curves prior to the glass transition temperature (T_g)

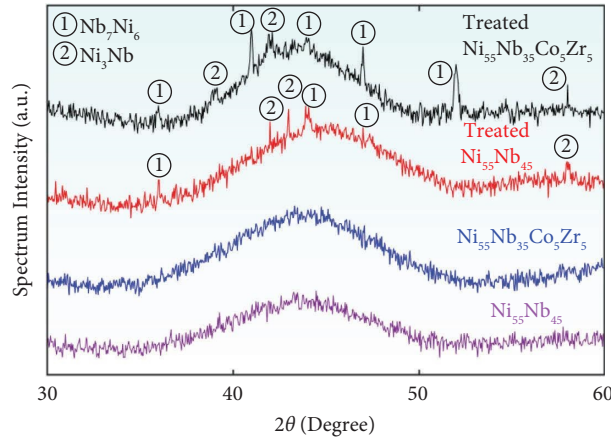


FIGURE 1: X-Ray diffraction patterns for raw and treated samples.

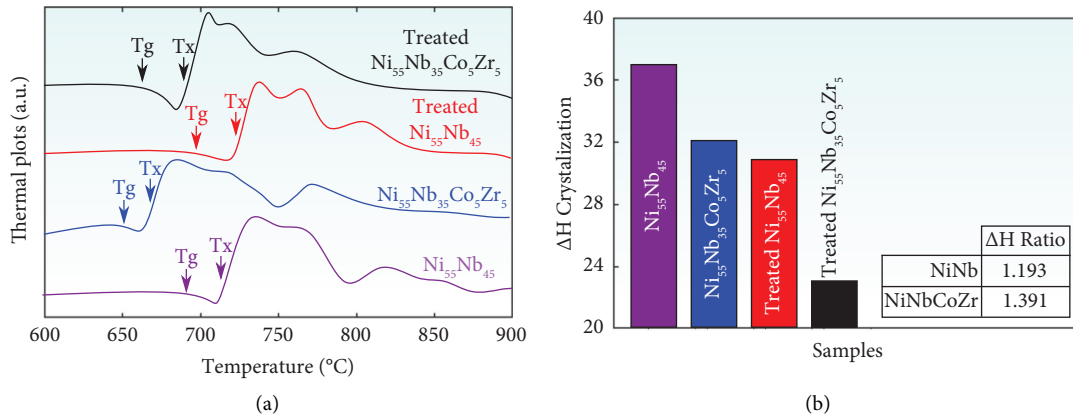


FIGURE 2: (a) thermographs of samples in the crystallization region for raw and treated samples, (b) enthalpy of crystallization for the samples.

up to the end of full crystallization. First of all, it is detected that the minor addition decreased the T_g value and thermal stability (ΔT_x) in the $Ni_{55}Nb_{35}Co_5Zr_5$ alloy (See Table 1). Moreover, compared to the BMG state, the thermo-mechanical process leads to a shift of crystallization peaks to the higher temperatures. The exothermic peaks of crystallization are also weakened, which is a sign of a decrease in the enthalpy of crystallization for the treated samples (See Figure 2(b)). This result is consistent with the formation of crystalline phases under thermomechanical processes, as also concluded from the XRD patterns. Considering the inset of Figure 2(b), the enthalpy ratio ($\Delta H_{\text{crys-untreated}}/\Delta H_{\text{crys-treated}}$) of $Ni_{55}Nb_{45}$ is lower than the $Ni_{55}Nb_{35}Co_5Zr_5$ system, approving that that of the crystallization under thermomechanical process is less pronounced in the $Ni_{55}Nb_{45}$ alloy.

Figure 3 demonstrates the polarization curves for all the samples. Based on the results, the i_{corr} for the amorphous $Ni_{55}Nb_{45}$ and $Ni_{55}Nb_{35}Co_5Zr_5$ are 0.07 and $0.11 \mu A \cdot cm^{-2}$, while their E_{corr} values are measured at 0.105 and $0.091 V_{\text{SCE}}$, respectively. This result indicates that the corrosion resistance of amorphous $Ni_{55}Nb_{45}$ is slightly better than that of $Ni_{55}Nb_{35}Co_5Zr_5$ BMG. However, both amorphous samples

TABLE 1: thermal parameters of samples.

Sample	T_g (°C)	T_x (°C)	ΔT_x (°C)
Treated $Ni_{55}Nb_{45}$	697	726	29
Untreated $Ni_{55}Nb_{45}$	691	719	28
Treated $Ni_{55}Nb_{35}Co_5Zr_5$	668	693	25
Untreated $Ni_{55}Nb_{35}Co_5Zr_5$	654	672	18

exhibit superior corrosion resistance compared to the stainless steel 316L with the i_{corr} and E_{corr} values of $10.7 \mu A \cdot cm^{-2}$ and $-0.25 V_{\text{SCE}}$. The polarization curves also reveal that the thermomechanical process leads to the conflicting effects on the corrosion behavior of amorphous alloys. For treated $Ni_{55}Nb_{45}$, the i_{corr} and E_{corr} values are $0.58 \mu A \cdot cm^{-2}$ and $-0.1 V_{\text{SCE}}$, respectively. This outcome implies that the crystallization induces the elemental partitioning and increases the anomalous chemical interfaces, leading to deterioration of corrosion resistance in the alloy [8]. On the other hand, the treated $Ni_{55}Nb_{35}Co_5Zr_5$ alloy shows excellent corrosion behavior with the i_{corr} and E_{corr} values of $0.05 \mu A \cdot cm^{-2}$ and $0.143 V_{\text{SCE}}$; however, this sample also includes the crystalline phases in its microstructure, as seen in Figure 1. The improvement of corrosion resistance in

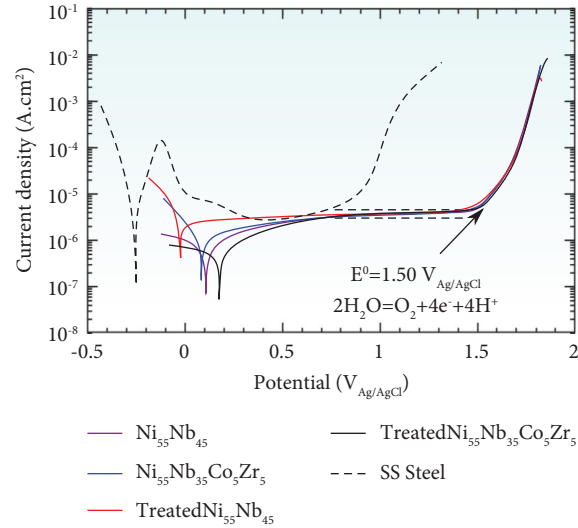


FIGURE 3: Potentiodynamic polarization curves of raw and treated samples in the condition simulated for proton exchange membrane fuel cell.

the treated $\text{Ni}_{55}\text{Nb}_{35}\text{Co}_5\text{Zr}_5$ can be associated to the minor addition of Co and Zr into the alloying composition, which will be discussed later. Another point in the polarization curves is the existence of a passivation plateau for all the samples with a current density in the range of $3.8\text{--}4.1\ \mu\text{A}\cdot\text{cm}^{-2}$. It is seen that the passive films exhibit a stable condition, while the water oxidation occurs near $+1.5\ \text{V}_{\text{Ag}/\text{AgCl}}$ [8], leading to rise of current density under the polarization. It is worth noting that the criterion for selecting an alloy as bipolar plates is to have i_{corr} less than $16\ \mu\text{A}\cdot\text{cm}^{-2}$ [26]. Hence, all of the samples, including the BMGs and their partially-crystalline states, meet the requirements for application in proton exchange membrane fuel cells.

Figure 4(a) illustrates the electrochemical impedance spectroscopy for the BMGs and their treated states. In general, the truncated feature of curves indicates high corrosion resistance, while the weak corrosion behavior of material can be defined by greater Z'/Z'' ratios. One can see that the results are consistent with that detected from the polarization curves. The treated $\text{Ni}_{55}\text{Nb}_{35}\text{Co}_5\text{Zr}_5$ exhibited the highest Z''/Z' ratio, meaning the best corrosion behavior among the samples. In the following, the $\text{Ni}_{55}\text{Nb}_{45}$ and $\text{Ni}_{55}\text{Nb}_{35}\text{Co}_5\text{Zr}_5$ BMGs showed the good corrosion resistance and finally the treated $\text{Ni}_{55}\text{Nb}_{45}$ with partially-crystalline state stands at the end of list. The spectroscopy result of stainless steel 316L is given in the inset of figure. To give a quantitative example, it can be estimated that the Z''/Z' ratio for the treated $\text{Ni}_{55}\text{Nb}_{35}\text{Co}_5\text{Zr}_5$ at Z' value of $0.05 \times 10^5\ \Omega\cdot\text{cm}^2$ is 12 times higher than the stainless steel, showing the superior corrosion resistance in the glassy systems. The graphs of the frequency response (Bode plot) for the samples are given in Figure 4(b). It is unveiled that the hot compression leads to increase of $|Z|$ value at the minimum of applied frequency for $\text{Ni}_{55}\text{Nb}_{35}\text{Co}_5\text{Zr}_5$, which is 9 times higher than its glassy state. On the other hand, the treated $\text{Ni}_{55}\text{Nb}_{45}$

exhibited a low $|Z|$ value (11 times smaller than its glassy state), showing that the thermomechanical process does not affect the corrosion behavior of amorphous alloys in the same way.

As described above, the response of BMGs to the hot compression strongly depends on the chemical compositions. In the $\text{Ni}_{55}\text{Nb}_{45}$ alloy, the treatment is accompanied with partial crystallization in the microstructure and the deterioration of corrosion resistance through the introduction of anomalous chemical interfaces. On the other hand, the hot deformation affects the $\text{Ni}_{55}\text{Nb}_{35}\text{Co}_5\text{Zr}_5$ BMG in a positive way so that the corrosion behavior improves compared with the glassy states. It is suggested that the presence of Zr and Co into the BMG is the main reason for this event. Zhang et al. [27] unveiled that the creation of a stable passivation layer can be expedited with the addition of cobalt to a Zr-based glassy alloy. Using the Co microalloying process on the high-entropy BMGs, it is found that the anticorrosion property significantly increases under the harsh marine environment [28]. Considering the ZrCuAl BMG, the Co minor addition depletes the copper in the surface film and decreases the corrosion current density [29]. Inoue et al. [7] also reported that the Zr addition into the NiNb glassy system declines the corrosion rate. Another investigation showed that the Zr addition to the NiNb BMG effectively decreases the metallic state Ni content in the surface films, leading to a reduction in passive current density in the corrosion test [30]. In our work, the hot deformation induces some NiNb crystalline constituents in the microstructure of $\text{Ni}_{55}\text{Nb}_{35}\text{Co}_5\text{Zr}_5$ BMG, leading to the enrichment of the glassy matrix from the Zr and Co, compared to the full glassy state. As a result, the effects of the minor addition were intensified, and the anticorrosion property was markedly improved in the $\text{Ni}_{55}\text{Nb}_{35}\text{Co}_5\text{Zr}_5$ alloy.

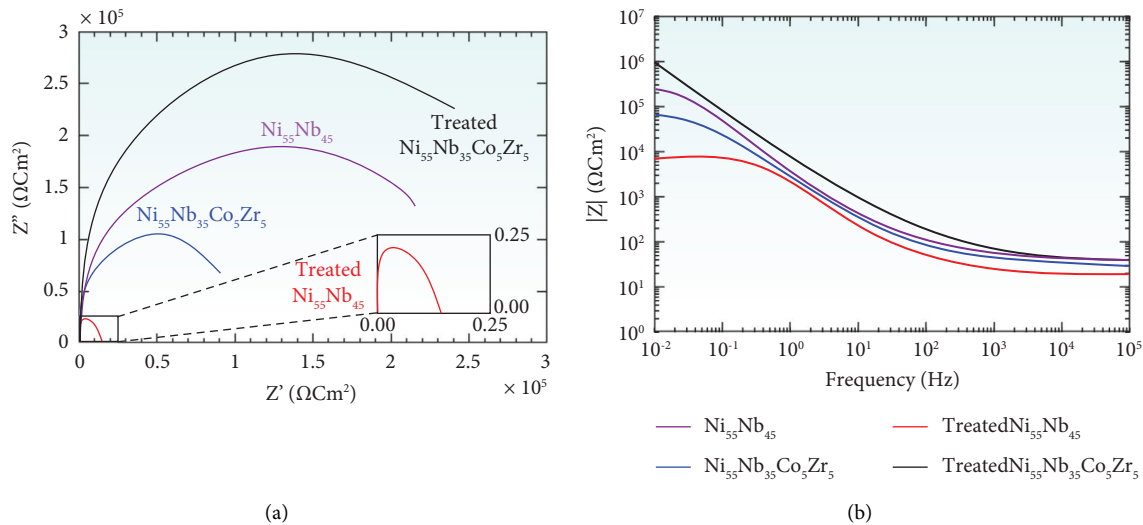


FIGURE 4: (a) EIS results of raw and treated samples, (b) the curves of $|Z|$ value as a function of Frequency.

4. Conclusion

The corrosion resistance of $\text{Ni}_{55}\text{Nb}_{45}$ and $\text{Ni}_{55}\text{Nb}_{35}\text{Co}_5\text{Zr}_5$ BMGs and their hot-compressed states was characterized in an environment similar to proton exchange membrane fuel cells. The main outcomes are as follows:

- (i) The XRD results demonstrated that the hot compression process led to formation of crystalline species, i.e., Ni_3Nb and Nb_7Ni_6 , in both of $\text{Ni}_{55}\text{Nb}_{45}$ and $\text{Ni}_{55}\text{Nb}_{35}\text{Co}_5\text{Zr}_5$ alloys; however, it was more pronounced in the $\text{Ni}_{55}\text{Nb}_{35}\text{Co}_5\text{Zr}_5$ sample.
- (ii) The DSC curves indicated that the Co and Zr minor additions decreased the T_g value and thermal stability (ΔT_x) of the NiNb-based alloy from 691°C and 28°C to 654°C and 18°C , respectively. Moreover, the thermomechanical process leads to the shift of crystallization peaks to the higher temperatures.
- (iii) The polarization test exhibited that the hot compression deteriorated the corrosion resistance of the $\text{Ni}_{55}\text{Nb}_{45}$ alloy through the introduction of anomalous chemical interfaces. On the other hand, the hot deformation affected the $\text{Ni}_{55}\text{Nb}_{35}\text{Co}_5\text{Zr}_5$ alloy in a positive way, so that the corrosion behavior improved compared with its fully glassy state. The quantitative analysis showed that the Z''/Z' ratio for the treated $\text{Ni}_{55}\text{Nb}_{35}\text{Co}_5\text{Zr}_5$ at Z' value of $0.05 \times 10^5 \Omega\cdot\text{cm}^2$ is 12 times higher than the stainless steel, showing the superior corrosion resistance in the glassy systems.

Data Availability

Data are available upon reasonable request to the corresponding author.

Conflicts of Interest

The authors declare that they have no conflicts of interest.

References

- [1] X. Han, S. Feng, S. Chen, Q. Cao, C. Zhang, and Q. Chen, "An investigation of Zr-based bulk metallic glasses as bipolar plates for proton exchange membrane fuel cells," *International Journal of Hydrogen Energy*, vol. 45, no. 4, pp. 3132–3144, 2020.
- [2] H. W. Yoon, J. Y. Choi, H. J. Park, J. H. Sun, S. Y. Shin, and K. I. Moon, "Zr-based thin-film metallic glass for bipolar plate in proton exchange membrane fuel cells," *Advanced Engineering Materials*, vol. 22, no. 10, Article ID 2000369, 2020.
- [3] N. Li, J. Pan, Z. Liu, and L. Liu, "Metallic glass nanostructures: forming strategies and functional applications," *Materials Today Advances*, vol. 15, Article ID 100253, 2022.
- [4] F. Bahrami, R. Amini, and A. H. Taghvaei, "Microstructure and corrosion behavior of electrodeposited Ni-based nanocomposite coatings reinforced with $\text{Ni}_{60}\text{Cr}_{10}\text{Ta}_{10}\text{P}_{16}\text{B}_4$ metallic glass particles," *Journal of Alloys and Compounds*, vol. 714, pp. 530–536, 2017.
- [5] Q. Li, S. S. Liu, X. H. Wang et al., "Mechanical and corrosion properties of Ti-Ni-Cu-Zr metallic glass matrix composites," *Journal of Alloys and Compounds*, vol. 727, pp. 1344–1350, 2017.
- [6] H. Joress, B. L. DeCost, S. Sarker et al., "A high-throughput structural and electrochemical study of metallic glass formation in Ni-Ti-Al," *ACS Combinatorial Science*, vol. 22, no. 7, pp. 330–338, 2020.
- [7] A. Inoue, T. Shimizu, S. Yamaura, Y. Fujita, S. Takagi, and H. Kimura, "Development of glassy alloy separators for a proton exchange membrane fuel cell (PEMFC)," *Materials Transactions*, vol. 46, no. 7, pp. 1706–1710, 2005.
- [8] G. Figueira, S. Dulnee, G. Y. Koga et al., "Influence of thermomechanical post-treatment on the corrosion behavior of $\text{Ni}_{57}\text{Nb}_{33}\text{Zr}_5\text{Co}_5$ bulk metallic glass," *Materials Letters*, vol. 288, Article ID 129350, 2021.
- [9] A. Espinoza Vazquez, A. Soriano Carranza, I. A. Figueroa Vargas, and F. Rodriguez, "Effect of the pH on the corrosion behaviour for a $\text{Ni}_{59.5}\text{Nb}_{40.5}$ binary metallic glass," *ECS Transactions*, vol. 106, no. 1, pp. 63–70, 2022.
- [10] K. Zhao, N. Wang, S. Li et al., "Corrosion behavior of $\text{Ni}_{62}\text{Nb}_{33}\text{Zr}_5$ bulk metallic glasses after annealing and cryogenic treatments," *ChemPhysMater*, 2022.

- [11] C. Poddar, J. Jayaraj, C. Mallika, and U. Kamachi Mudali, "Oxidation behaviour of Ni60Nb30Ta10 metallic glass below its glass transition temperature," *Journal of Alloys and Compounds*, vol. 728, pp. 1146–1152, 2017.
- [12] C. Poddar, J. Jayaraj, and S. Ningshen, "Passive film characteristics and corrosion behavior of thermally oxidized Ni60Nb30Ta10 metallic glass in nitric acid medium," *Journal of Alloys and Compounds*, vol. 783, pp. 680–686, 2019.
- [13] C. Poddar, S. Ningshen, and J. Jayaraj, "Corrosion assessment of Ni60 Nb30Ta10 metallic glass and its partially crystallized alloy in concentrated nitric acid environment," *Journal of Alloys and Compounds*, vol. 813, Article ID 152172, 2020.
- [14] L. Jiang, Z. Q. Chen, H. B. Lu et al., "Corrosion protection of NiNb metallic glass coatings for 316SS by magnetron sputtering," *Journal of Materials Science and Technology*, vol. 79, pp. 88–98, 2021.
- [15] C. Poddar, J. Jayaraj, S. Amirthapandian, and S. Ningshen, "Effect of thermally grown amorphous oxide film on the corrosion resistance properties of Ni50Zr25Nb25 metallic glass in nitric acid medium," *Intermetallics*, vol. 113, Article ID 106571, 2019.
- [16] Z. M. Wang, J. Zhang, X. C. Chang, W. L. Hou, and J. Q. Wang, "Structure inhibited pit initiation in a Ni–Nb metallic glass," *Corrosion Science*, vol. 52, no. 4, pp. 1342–1350, 2010.
- [17] Z. F. Wu, Q. P. Cao, Y. Ma et al., "Thickness-dependent pitting corrosion behavior in Ni–Nb thin film metallic glass," *Thin Solid Films*, vol. 564, pp. 294–298, 2014.
- [18] K. Zhang, X. Gao, Y. Dong, Q. Xing, and Y. Wang, "Effect of annealing on the microstructure, microhardness, and corrosion resistance of Ni62Nb33Zr5 metallic glass and its composites," *Journal of Non-crystalline Solids*, vol. 425, pp. 46–51, 2015.
- [19] R. Wang, Y. Wang, J. Yang, J. Sun, and L. Xiong, "Influence of heat treatment on the mechanical properties, corrosion behavior, and biocompatibility of Zr56Al16Co28 bulk metallic glass," *Journal of Non-crystalline Solids*, vol. 411, pp. 45–52, 2015.
- [20] X. Zhao, J. Sun, M. Yu et al., "Effects of heat treatment on the thermal, mechanical and corrosion properties of deformed Zr-based bulk metallic glasses," *Materials Chemistry and Physics*, vol. 256, Article ID 123705, 2020.
- [21] G. Perumal, H. S. Grewal, A. Ayyagari, S. Mukherjee, and H. S. Arora, "Enhancement in bio-corrosion resistance of metallic glass by severe surface deformation," *Applied Surface Science*, vol. 487, pp. 1096–1103, 2019.
- [22] Q. Xing, K. Zhang, Y. Wang et al., "Effects of pre-compression on the microstructure, mechanical properties and corrosion resistance of RE65Co25Al10 (RE = Ce, La, Pr, Sm and Gd) bulk metallic glasses," *Intermetallics*, vol. 67, pp. 94–101, 2015.
- [23] L. Duclos, M. Lupsea, G. Mandil, L. Svecova, P.-X. Thivel, and V. Laforest, "Environmental assessment of proton exchange membrane fuel cell platinum catalyst recycling," *Journal of Cleaner Production*, vol. 142, pp. 2618–2628, 2017.
- [24] W. J. Song, H. Chen, H. Guo, F. Ye, and J. R. Li, "Research progress of proton exchange membrane fuel cells utilizing in high altitude environments," *International Journal of Hydrogen Energy*, vol. 47, no. 59, pp. 24945–24962, 2022.
- [25] H. Wang, M. A. Sweikart, and J. A. Turner, "Stainless steel as bipolar plate material for polymer electrolyte membrane fuel cells," *Journal of Power Sources*, vol. 115, no. 2, pp. 243–251, 2003.
- [26] B. D. Cunningham and D. G. Baird, "Development of bipolar plates for fuel cells from graphite filled wet-lay material and a compatible thermoplastic laminate skin layer," *Journal of Power Sources*, vol. 168, no. 2, pp. 418–425, 2007.
- [27] Y. Zhang, L. Yan, X. Zhao, and L. Ma, "Enhanced chloride ion corrosion resistance of Zr-based bulk metallic glasses with cobalt substitution," *Journal of Non-crystalline Solids*, vol. 496, pp. 18–23, 2018.
- [28] S. Zhang, Z. Zhang, P. He, Y. Gao, and X. Liang, "Effect of Co addition on the microstructure, thermal stability and anti-corrosion properties of AlNiZrYCo high-entropy metallic glass ribbons," *Journal of Non-crystalline Solids*, vol. 585, Article ID 121555, 2022.
- [29] W. Zhou, W. P. Weng, and J. X. Hou, "Glass-forming ability and corrosion resistance of ZrCuAlCo bulk metallic glass," *Journal of Materials Science and Technology*, vol. 32, no. 4, pp. 349–354, 2016.
- [30] D. Li, Z. Zhu, H. Zhang, A. Wang, and Z. Hu, "The influence of Zr substitution for Nb on the corrosion behaviors of the Ni-Nb-Zr bulk metallic glasses," *Science China Physics, Mechanics and Astronomy*, vol. 55, no. 12, pp. 2362–2366, 2012.